Atmospheric Environment 264 (2021) 118684

Contents lists available at ScienceDirect

Atmospheric Environment

journal homepage: www.elsevier.com/locate/atmosenv

MODIS high-resolution MAIAC aerosol product: Global validation and analysis

Wenmin Qin [a,*], Hejin Fang [a,1], Lunche Wang [a,**], Jing Wei [b], Ming Zhang [a], Xin Su [a], Muhammad Bilal [c], Xun Liang [a]

[a] Hunan Key Laboratory of Remote Sensing of Ecological Environment in Dongting Lake Area, School of Geography and Information Engineering, China University of Geosciences, Wuhan, China
[b] Department of Chemical and Biochemical Engineering, Iowa Technology Institute, Center for Global and Regional Environmental Research, University of Iowa, USA
[c] School of Marine Science, Nanjing University of Information Science & Technology, Nanjing, China

HIGHLIGHTS

- MODIS MAIAC 1 km resolution AOD products are evaluated globally.
- The spatial continuity of MAIAC AOD retrievals during 2000–2019 are illustsrated.
- Retrievals errors related to varying surface and atmospheric conditions are analyzed.
- The spatial and temporal variations of AOD values over the world are investigated.

ARTICLE INFO

Keywords:
MAIAC
MODIS
AOD
1 km resolution
Global
Validation

ABSTRACT

This paper attempt to verify the accuracy of the Multi-Angle Implementation of Atmospheric Correction (MAIAC) aerosol optical depth (AOD) product on a global scale using AOD measurements during 2000–2019 at 332 Aerosol Robotic Network (AERONET) sites. The results indicate that MAIAC AOD retrievals are highly correlated with ground-based AOD measurements. The correlation coefficients (R) are greater than 0.8 at more than 68% of AERONET sites. Meanwhile, the performance of MAIAC AOD retrievals in different climate zones is also investigated. The accuracy of MAIAC AOD retrievals is high (within expected error (EE) = 87.49% and 83.15%) in the regions of tropical rainforest climate and tropical open forest climate. Then, the uncertainties and estimation deviation of MAIAC AOD retrievals in various land-cover-types are analyzed. The results find that the MAIAC AOD retrievals show high correlation with aerosol measurements in the forest (within EE > 95%), while the poor accuracy is always observed in the barren areas (within EE = 62.56%, RMSE = 0.12). The uncertainty of the MAIAC AOD retrievals is not only related to the satellite and solar geometries, but also depends on the aerosol conditions, which become larger with the increase of aerosol loading and Ångstrom exponent (AE). Finally, the spatial variations of AOD values over the world are investigated. High AOD values are mainly distributed in Central Africa, Saudi Arabia, Southern Asia and China.

1. Introduction

Atmospheric aerosols are the multi-phase system composed of solid and liquid particles suspended in the atmosphere. It comes from natural processes such as volcanic eruption, wildfire and sand dust over land, and also from human activities such as biomass combustion, fossil combustion and industrial pollution (Ramanathan and Ramana, 2005). Although the volume of aerosols is small, the aerosol direct radiation effect and the aerosol-cloud indirect effect have profound influences on the transmission of solar energy in the atmosphere, thus affecting the

* Corresponding author. Hunan Key Laboratory of remote sensing of ecological environment in Dongting Lake Area, School of Geography and Information Engineering, China University of Geosciences, Lumo road 388, Hongshan District, Wuhan, 430074, China.
** Corresponding author.
E-mail addresses: qinwenmin@cug.edu.cn (W. Qin), wang@cug.edu.cn (L. Wang).
[1] Co first author.

https://doi.org/10.1016/j.atmosenv.2021.118684
Received 17 June 2021; Received in revised form 27 July 2021; Accepted 13 August 2021
Available online 20 August 2021

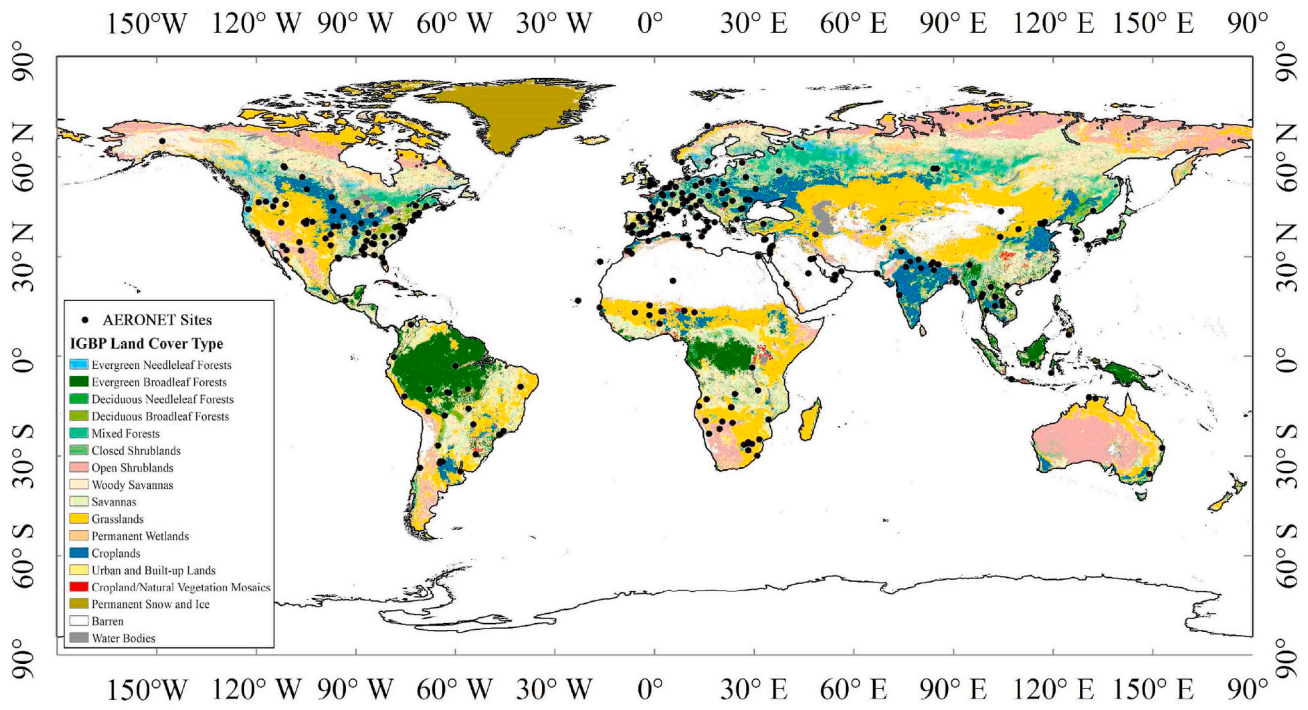

Fig. 1. The distribution of AERONET sites in different land-cover-types.

Table 1
Detailed information about the MODIS land-cover-types used in this study.

Number	Specific class
a	Evergreen Needleleaf Forests
b	Evergreen Broadleaf Forests
c	Deciduous Broadleaf Forests
d	Mixed Forests
e	Open Shrublands
f	Woody Savannas
g	Savannas
h	Grasslands
i	Croplands
j	Cropland/Natural Vegetation Mosaics
k	Urban and Built-up Lands
l	Barren

Earth's energy budget (Seinfeld et al., 2016; Mhawish et al., 2017). Moreover, aerosol particles with a diameter of 10 μm and 2.5 μm or less are inhalable particles, which can endanger human health (Banerjee et al., 2017; Evans et al., 2013; Kumar et al., 2015; Pope et al., 2002; Wei et al., 2021). Therefore, it is necessary to analyze the characteristics of aerosols and monitor the spatial and temporal variations of aerosols (Kaufman et al., 2002). Aerosols have the following characteristics: complex types, diverse sources, wide distribution and uneven distribution, which bring great uncertainty to climate research. The development of ground aerosol observation networks fills in this gap. For example, the Aerosol Robotic Network (AERONET) could provide long-term and global ground-based aerosol observations (Holben et al., 2001). However, these ground observation sites are still too sparse for aerosol research and applications needing AOD records with high resolution and continuity. Satellite remote sensing can overcome this problem, which could provide long-term global aerosol data (Kaufman et al., 2002), making it possible to investigate the aerosol properties in regional and global scales (Emili et al., 2011).

Satellite sensors (e.g., Moderate-resolution Imaging Spectroradiometer (MODIS) (Kaufman et al., 1997), Multi-angle Imaging Spectro Radiometer (MISR) (Kahn et al., 2010), Visible Infrared Imaging Radiometer Suite (VIIRS) (Jackson et al., 2013), Advanced Baseline Imager (ABI) (Zhang et al., 2020) and Advanced Himawari Imager (AHI) (Su et al., 2021; Yoshida et al., 2018) can provide continuous records of aerosol optical properties over large areas. Among these satellite sensors, MODIS aerosol products are the most widely used products in regional and global scales. MODIS aerosol retrievals are mainly produced based on three algorithms: Dark target (DT), Deep blue (DB) and MAIAC algorithms. The limitation of DT algorithm is that it can't retrieve aerosol optical properties from bright surface (e.g., part of the urban, desert and Gobi, etc) (Hsu et al., 2004). However, DB algorithm assumes that the short-wave infrared band is completely transparent for vegetation area; the errors are prone to occur when the AOD loading is high.

Lyapustin (2011) developed the MAIAC algorithm for retrieving AOD values over bright and dark surface at 1 km resolution using MODIS products (Lyapustin et al., 2018). MAIAC algorithm can provide more refined aerosol characteristics and meet the requirements for regional aerosol monitoring in more fine spatial scales (Tao et al., 2019). At present, many scholars have evaluated the quality and potential of the MAIAC AOD product in different regions, or made relevant research on this product. Tao et al. (2019) found that the MAIAC algorithm was systematically underestimated in the desert areas in western China, while in eastern China, a positive bias was found at low-moderate aerosol loading. Zhang et al. (2019) showed that the accuracy of MAIAC algorithm was closely correlated to the land-cover-types, aerosol loading and aerosol size in China. Mhawish et al. (2019) indicated that MAIAC AOD product performed well in South Asia, and the accuracy of MAIAC AOD product was better than DT and DB AOD products. Superczynski et al. (2017) verified that the MAIAC AOD products performed well in South America and North America. Lee et al. (2017) found that MAIAC AOD product and AERONET site data have a better correspondence in arid areas of the Dead sea. Chudnovsky et al. (2013) found that MAIAC AOD product could capture the spatial variations of PM2.5 with higher accuracy than that of MYD04. Emili et al. (2011) analyzed the accuracy and potential of MAIAC AOD in the alpine region, and concluded that the terrain is related to the average aerosol distribution. In all, the MAIAC AOD products have been evaluated in different climate zones and terrain in different area around the world, but few

Table 2
Division and definition criteria of the Köppen climate zone (Peel et al., 2007).

Climatic zone	Climatic type	Climate subtype	characteristic
A: Equatorial zone			$T_{cold} \geq 18$
	Af (Tropical rainforest climate)		$P_{dry} \geq 60$ mm
	Aw (Tropical open forest climate)		Pdry≤60 mm & Pdry≥ (100-MAP/25) mm
	Am (tropical monsoon climate)		Pdry≤60 mm & Pdry≤ (100-MAP/25) mm
B: Arid zone			MAP<10 P_{th}
	BS (Steppe climate)		MAP≥5 P_{th}
	BW (Desert climate)		MAP<5 P_{th}
		h	MAT≥18 °C
		k	MAT < 18 °C
C: Warm zone			T_{hot}>10 °C & 0 °C < T_{cold}<18 °C
	Cs (Dry summer and warm climate)		P_{sdry}<40 mm & P_{sdry} < P_{wwet}/3
	Cw (Dry and warm climate in winter)		P_{wdry} < P_{swet}/10
	Cf (Normally humid and warm climate)		Neither Cw nor Cf
		a	$T_{hot} \geq 22$ °C
		b	Thot < 22 °C & count (Tmon > 10 °C) ≥4
		c	Tcold ≥ −38 °C & count (Tmon > 10 °C) < 4
D: Cold temperate zone			T_{hot}>10 °C & $T_{cold} \leq 0$ °C
	Df (Normally humid and cold temperature climate)		$P_{wdry} \geq P_{swet}/10$
	Dw (Sub-frigid monsoon climate)		$P_{wdry} \geq P_{swet}/10$
	Ds (Subarctic continental climate)		
		a	$T_{hot} \geq 22$ °C
		b	Thot < 22 °C & count (Tmon > 10 °C) ≥4
		c	Tcold ≥ −38 °C & count (Tmon > 10 °C) < 4
		d	Tcold < -38 °C
E: Polar zone			T_{hot}<10 °C
	EF (Tundra climate)		$T_{hot} \geq 0$ °C
	ET (Ice climate)		T_{hot}< 0 °C
		G	H ≥ 2500 m

*T_{cold} = the average temperature of the coldest month, T_{hot} = the average temperature of the hottest month, P_{dry} = the driest monthly precipitation, P_{sdry} = the driest monthly precipitation in summer (April to September), P_{wdry} = the driest monthly precipitation in winter (October to March), P_{swet} = the wettest monthly precipitation in summer, P_{wwet} = the wettest monthly precipitation in winter. MAP = the annual precipitation, MAT = the annual average temperature, P_{th} = if the regional summer precipitation is greater than or equal to 70% of MAP, then $P_{th} = 2$ (MAT + 14) mm; if the regional winter precipitation is greater than or equal to 70% of the annual precipitation, then P_{th} = 2MAT mm; if it is less than the above proportion, then $P_{th} = 2$ (MAT + 7) mm.

studies have been conducted to verify its accuracy and robustness on a global scale.

This study attempts to evaluate the accuracy of MAIAC AOD retrievals using AOD observations during 2000–2019 at 332 global AERONET sites in various climate zones, land-cover-types and aerosol conditions. Meanwhile, the spatial and temporal variations of MAIAC AOD product over the world are also investigated. Below, section 2 introduces the data used, verification metrics and analysis approaches. Section 3 describes the continuity and uncertainties of MAIAC AOD product, and analyzes the spatiotemporal variations. Section 4 provides a summary of the main result. This study may help readers have a preliminary understanding and performance assessment of MODIS MAIAC AOD product at a global scale.

Table 3
Description of the dataset used in this study.

Source	Scientific Data Set Name	Parameters	Resolution
AERONET	Version 3, Level 2	Aerosol Optical Depth & AE (440 nm–675nm)	15 min/Sites
MODIS	MCD12Q1	Land-cover-types	Instantaneous/ 500 m
MODIS C6.0	MCD19A2	Optical_Depth_550	Instantaneous/1 km
MODIS C6.0	MCD19A2	Cosine of solar zenith angle (cosSZA) Cosine view zenith angle (cosVZA) Relative azimuth angle (RelAZ) Scattering angle	Instantaneous/5 km

2. Data and method

2.1. AERONET data

AERONET (https://aeronet.gsfc.nasa.gov) is a global aerosol monitoring network organized by the National Aeronautics and Space Administration (NASA) (Holben et al., 1998). AERONET version 3 provides optical and physical properties of aerosols, and released three quality levels of aerosol observations, i.e., level 1.0 (unscreened), level 1.5 (cloud mask) and level 2.0 (cloud mask and quality control) (Holben et al., 2001; Smirnov et al., 2000). In this study, the aerosols observations are obtained from 332 AERONET sites. AERONET does not directly provide observations at 550 nm, the Ångström index for the wavelength of 440 nm–675nm is used to interpolate the AOD Ångström index at 550 nm (α), and then the AOD (550 nm) were obtained using the following formula (Ångström, 1929) :

$$\alpha \cdot = \cdot - \frac{\ln(\tau_{440}/\tau_{675})}{\ln(440/675)} \quad (1)$$

$$\tau_{550} = \tau_{440}\ (550/440)^{-\alpha} \quad (2)$$

2.2. MODIS MAIAC AOD product

The MAIAC algorithm is used for retrieve AOD over land, which uses time series to separate the contribution of aerosol and land reflection, and also considers the effects of bidirectional surface reflectivity (Lyapustin et al., 2018). The time series analysis and image-based processing techniques are used in MAIAC algorithm to perform aerosol retrieval and atmospheric correction in the brighter surface and dark vegetation land (Lyapustin et al., 2011, 2018). The MAIAC algorithm adds smoke (dust) detection capabilities, improves cloud and snow cover and enhances aerosol retrieval on bright surface (Lyapustin et al., 2012). Compared with DT and DB AOD product, MAIAC AOD product has higher spatial coverage and retrieval frequency. The high spatial resolution of MAIAC AOD retrievals improves the ability to determine the characteristics of fine aerosols and distinguish aerosol sources (Mhawish et al., 2019).

2.3. Auxiliary data

The land-cover-types were derived from MODIS MCD12Q1 product with a spatial resolution of 500 m (see Fig. 1). In this study, the accuracy of the MAIAC AOD product is evaluated on different underlying surfaces. By matching the MODIS land-cover-types product with the AERONET site, remaining 12 land-cover-types were successfully matched (Table 1). Four geometric angles including the Viewing Zenith Angle

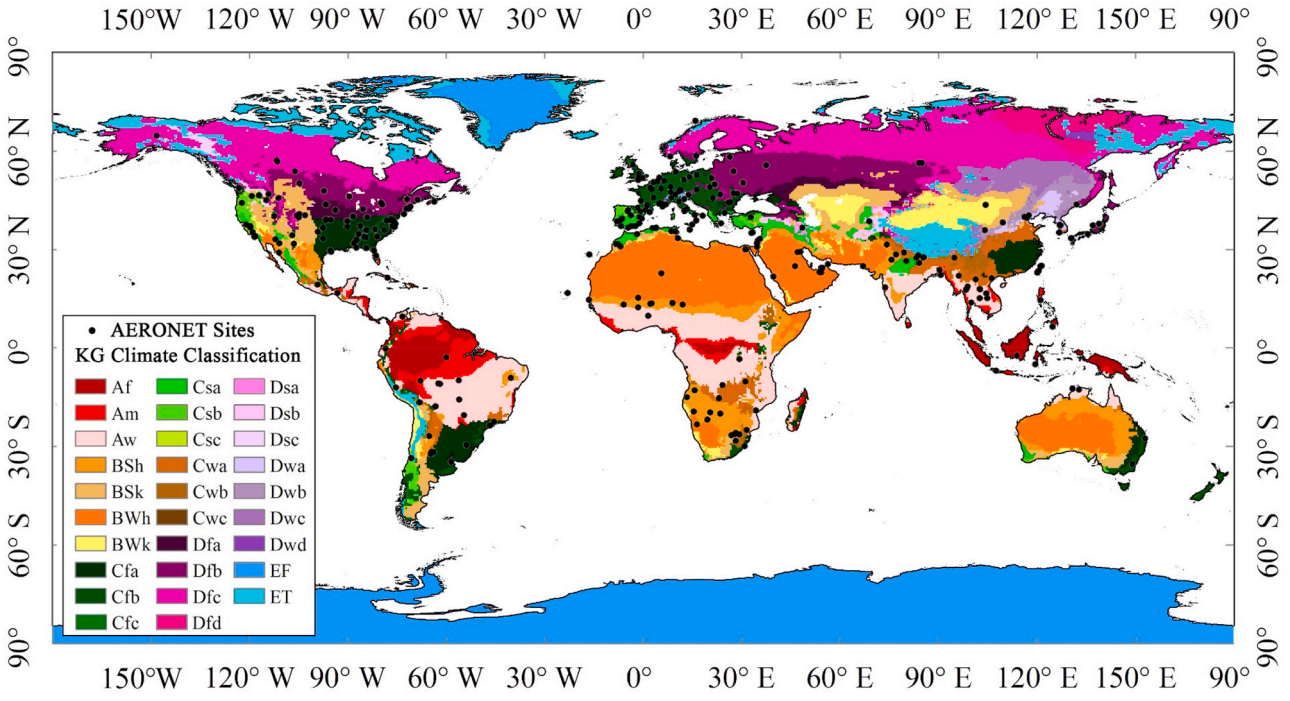

Fig. 2. Distribution of AERONET sites in Köppen climate subtype zone.

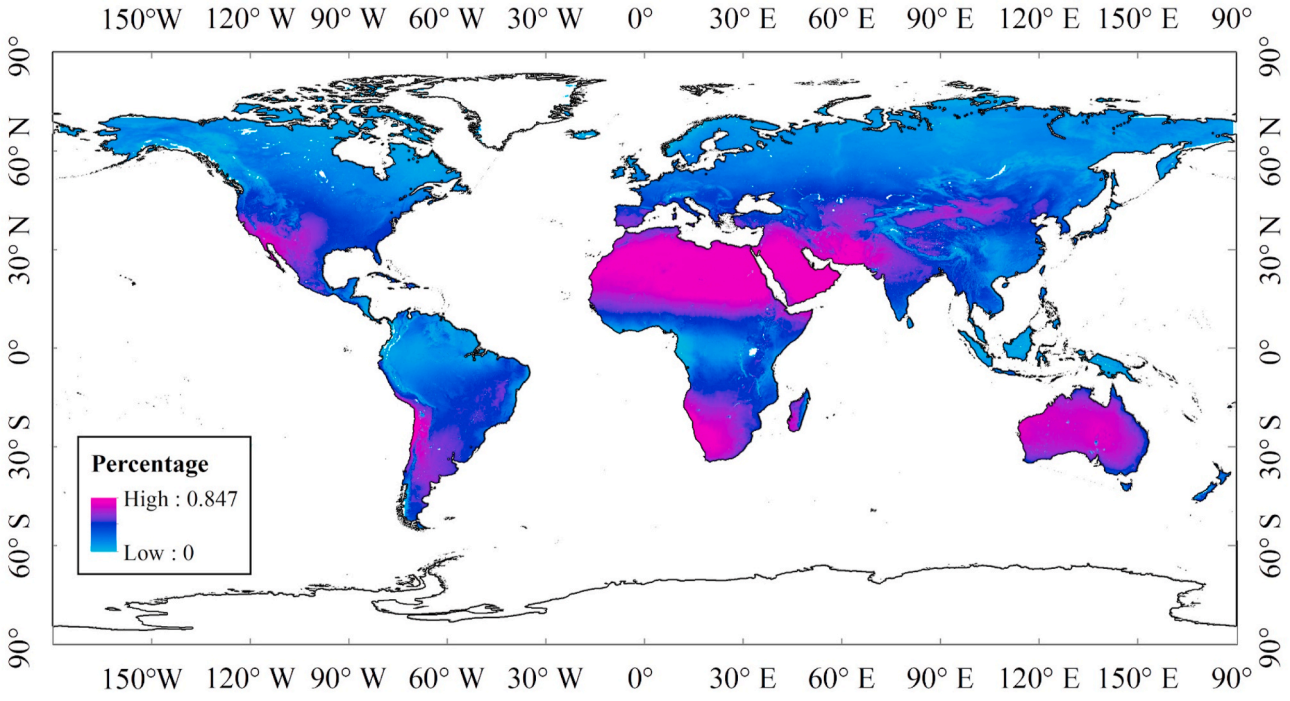

Fig. 3. Global spatial continuity of MAIAC AOD product from 2000 to 2019.

(VZA), Solar Zenith Angle (SZA), Scattering angle (SA) and Relative Azimuth Angle (RAA) are obtained from MCD19A2. Meanwhile, the accuracy of MAIAC AOD values is also analyzed in different Köppen climate zones around the world. As the most widely used climate classification, the Köppen climate zones divided world continent into five major climate zones (A, B, C, D, E). Then, the monthly and annual temperature and the seasonal variation of rainfall are also considered in each zone. Finally, according to the distribution of vegetation, several climatic types are determined (Table 2) (Gengrui and Yu, 2015; Peel et al., 2007). The distribution of the selected AERONET sites in different Köppen climate zones (29 climate subtypes) is shown in Fig. 2 (see Table 3).

2.4. Evaluation and analysis methods

In this study, a 1 km * 1 km pixel window was utilized to extract the single pixel value of MAIAC AOD values corresponding to the AERONET sites. A ±30 min instantaneous window was selected for screening

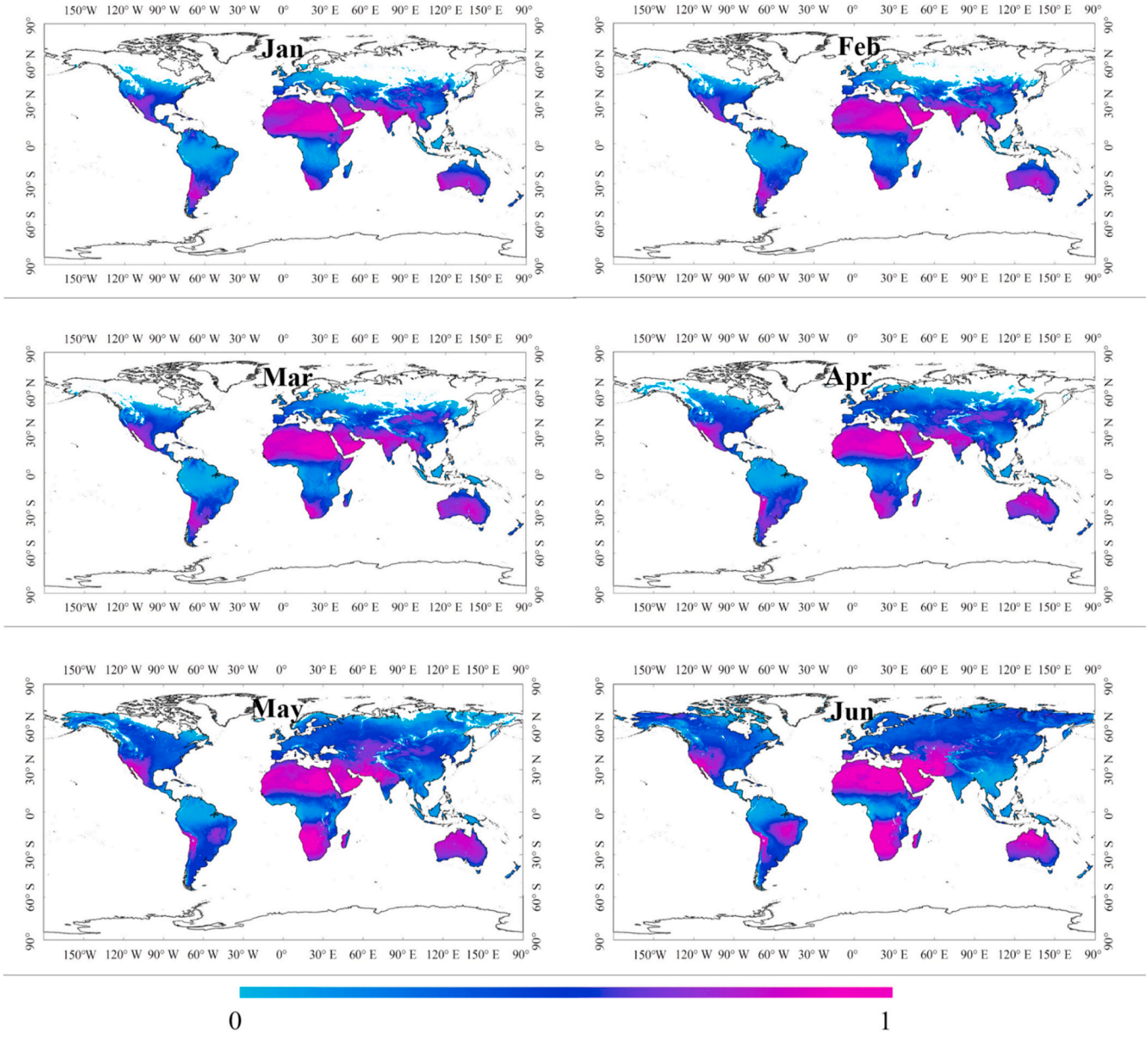

Fig. 4. Monthly average spatial continuity of MAIAC AOD product.

AERONET data based on the satellite transit and data acquisition time. After the AERONET data was matched with the satellite data, this study used the expected error (EE) to evaluate the quality of the MAIAC AOD product, which was calculated as EE = ± (0.05 + 0.15 AOD) (Levy et al., 2013).

Meanwhile, the correlation coefficient (R), root mean square error (RMSE), mean absolute error (MAE) and mean absolute difference (MAD) were also used to validate the accuracy of MAIAC AOD product.

$$RMSE = \sqrt{\frac{\sum_{i=1}^{M}\left(X_{pi} - X_{oi}\right)^2}{M}} \tag{3}$$

$$MAE = \frac{1}{M}\sum_{i=1}^{M}\left|X_{pi} - X_{oi}\right| \tag{4}$$

$$\boldsymbol{MAD} = (100 / \ \boldsymbol{X_{om}})\frac{1}{\boldsymbol{M}}\sum_{i=1}^{\boldsymbol{M}}\left|\boldsymbol{X_{pi}} - \boldsymbol{X_{oi}}\right| \tag{5}$$

$$R = \frac{\sum_{i=1}^{M}\left(X_{pi} - X_{pm}\right)\left(X_{oi} - X_{om}\right)}{\sqrt{\sum_{i=1}^{M}\left(X_{pi} - X_{pm}\right)^2\sum_{i=1}^{M}\left(X_{oi} - X_{om}\right)^2}} \tag{6}$$

where i is the number of the selected AERONET sites, X_{oi} is observed data and X_{pi} is MODIS MAIAC AOD data. M is the sample number. X_{om} and X_{pm} represent the mean of the observed and retrieved values, respectively.

3. Result and analysis

3.1. Global spatial continuity of MAIAC AOD product

The MAIAC algorithm could retrieve aerosols in dense vegetation coverage areas and bright surfaces. Meanwhile, it combines the cloud mask (CM) algorithm based on spatiotemporal analysis to enhance the ability of cloud detection (Lyapustin et al., 2008). Therefore, the MAIAC algorithm could provide AOD records with higher continuity. Fig. 3 shows the spatial continuity of MAIAC AOD products from 2000 to

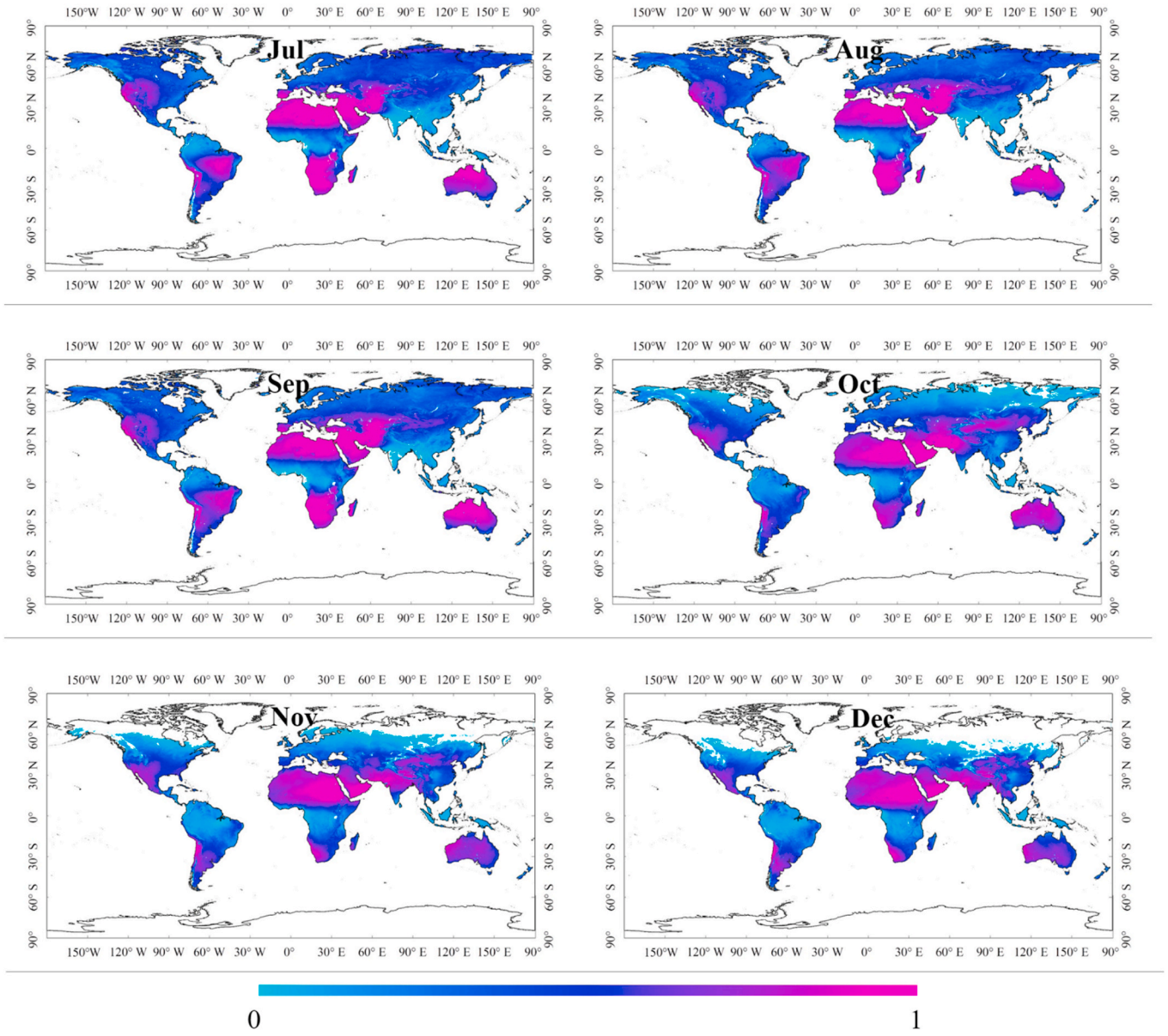

Fig. 5. Monthly average spatial continuity of MAIAC AOD product.

2019. The aerosol retrievals continuity is relatively better in Oceania, Saudi Arabia and surrounding areas, northern and southern Africa, western United States and Argentina. The MAIAC algorithm does not retrieve AOD over snow. Thus, the continuity of aerosol retrieval is generally poor in areas above 45°N in the northern hemisphere owing to perennial snow in winter. Especially in the Polar regions of the northern hemisphere, the AOD records are seriously missing due to the perennial snow cover. The spatial continuity of the MAIAC AOD records is also poor in Equatorial region, because of the frequent rainy weather and cloud occurrences there.

Fig. 4 and Fig. 5 show the monthly average spatial continuity of MAIAC AOD product. Interestingly, the spatial continuity of MAIAC AOD product changes with seasons. The continuity of high latitudes in the northern hemisphere is seriously absent in December, January and February (DJF). The reason is that there is snow all year round, and the MAIAC algorithm does not retrieve AOD over snow. It is obvious that the percentage of effective observation records increased (e.g., area above 45°N in the northern hemisphere, Oceania, northern South America and northern Africa) from March to May (MAM) and from June to August (JJA). But in September, October and November (SON), the percentage of effective observation records decrease, especially in the northern hemisphere. In the southern hemisphere, the continuity is good in most areas, especially in Oceania.

3.2. *Validation with ground AOD observations*

Fig. 6 illustrates the validation results of MAIAC AOD retrievals against the AOD observations at 332 AERONET sites from 2000 to 2019. The results indicate a significant heterogeneity of the performances of MAIAC AOD retrievals. The MAIAC AOD retrievals have a high correlation with the ground-based measurements. The R is higher than 0.8 at more than 69% of the sites, and lower than 0.5 at only 4 sites. In general, MAIAC AOD product performs well in Oceania, eastern North America and Europe. These areas are mostly covered by typical dark surface and dense vegetation, which is conducive to aerosol retrievals (Wei et al., 2018). By contrast, relatively poor accuracy of MAIAC AOD retrievals is found in southwest North America, because the southwest North America is mostly desert area (bright surfaces), and the low sensitivity of top of the atmosphere (TOA) reflectivity to the aerosol changes leading to the high uncertainty of bright surfaces. The accuracy of MAIAC AOD

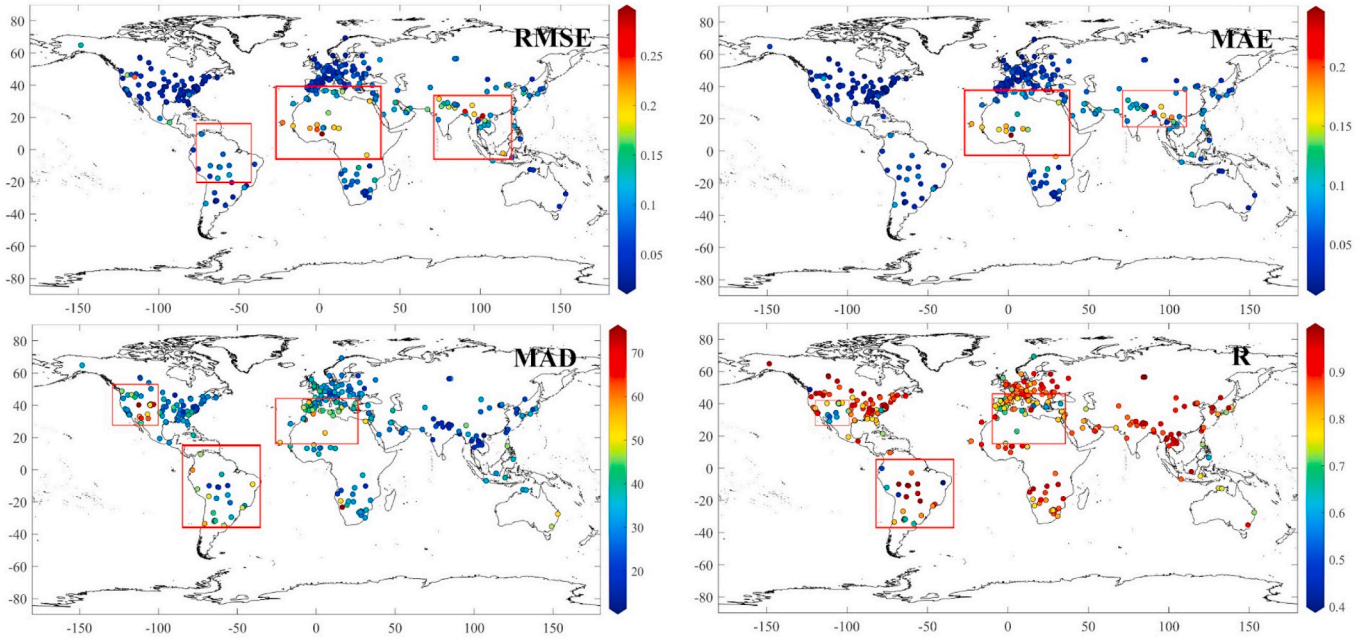

Fig. 6. The spatial variations of the RMSE, MAE, MAD (%) and R for MAIAC AOD values.

Table 4
Statistical indicators in different Köppen climate type zones.

Climate	N	RMSE	MAE	R	EE (%)	>EE	<EE	Slope	Intercepts
Af	2821	0.08	0.04	0.87	87.49	7.02	5.49	0.95	0.00
Am	5674	0.09	0.06	0.89	78.55	15.62	5.83	1.01	−0.03
Aw	7115	0.08	0.05	0.89	83.15	12.04	4.81	0.85	0.00
BS	11005	0.12	0.08	0.85	68.45	21.64	9.91	0.75	0.02
BW	6924	0.08	0.05	0.84	80.46	11.76	7.78	0.76	0.02
Cf	35252	0.05	0.07	0.92	73.87	18.36	7.77	0.83	0.01
Cs	18242	0.07	0.08	0.89	69.22	21.82	8.96	0.84	0.00
Cw	6137	0.07	0.05	0.89	79.73	14.16	6.11	0.77	0.01
Df	10248	0.09	0.06	0.88	73.99	17.93	8.09	0.74	0.02
Ds	511	0.10	0.08	0.85	55.19	35.62	9.20	0.77	0.00
Dw	2770	0.08	0.06	0.95	78.59	18.66	2.74	0.84	−0.01
EF	147	0.14	0.05	0.97	85.03	12.93	2.04	1.20	−0.05
ET	1864	0.12	0.05	0.79	80.20	11.35	8.45	0.54	0.04

retrievals is also poor in central South America, owing to the uncertainty of satellite signals caused by the cloudy and rainy weather there.

3.2.1. Regions-scale performance in different climatic

Table 4 shows the validation results of MAIAC AOD retrievals in different climatic zones. The satisfactory percentage of the matchup points falling within the EE envelope (within EE = 87.49%, 83.15% and 80.46%, respectively) are found in the Af, Aw and BW. The RMSE for Af, Aw and BW all are 0.08; the MAE are 0.04, 0.05 and 0.05. However, the MAIAC AOD retrievals are most significantly overestimated in D_S with large deviations (>EE = 35.62%, RMSE = 0.1, MAE = 0.08 and slope = 0.77). Because the lime soil is the most widely distributed in Ds which is not conducive to the aerosol retrievals. The obvious overestimation phenomenon also appears in BS and Cs (>EE = 21.64% and 21.82%). The small number of samples (N) results in a good EE in the polar climate (EF, ET) zones. In general, MAIAC AOD product performs poor with great deviations (RMSE = 0.14 and 0.12) in the polar climate zones. Because the polar climate (EF, ET) regions are covered with snow all the year round which makes it difficult to retrieve aerosols.

3.2.2. Land-cover-scale performance

Fig. 7 shows the verification indexes of MAIAC AOD retrievals under different land-cover-types. Generally, the MAIAC AOD retrievals and AERONET observations have high correlation under different land-cover-types with mean R value of 0.88. The results indicate that MAIAC AOD retrievals have satisfactory reliability in the areas covered with dense evergreen forest, such as, evergreen needleleaf forests (Fig. 7a), deciduous broadleaf forests (Fig. 7c) and mixed forests (Fig. 7d) . MAIAC AOD retrievals have high matchup points within EE (EE > 95%), and the overall AOD retrievals accuracy is stable, with small deviation (RMSE <0.07 and MAE <0.04) in the above three land-cover-types. Similar results are found in woody grasslands (Fig. 7f). Because evergreen surface provides stability and powerful spectral regression coefficient (SRC) retrieved capabilities, thereby enhancing

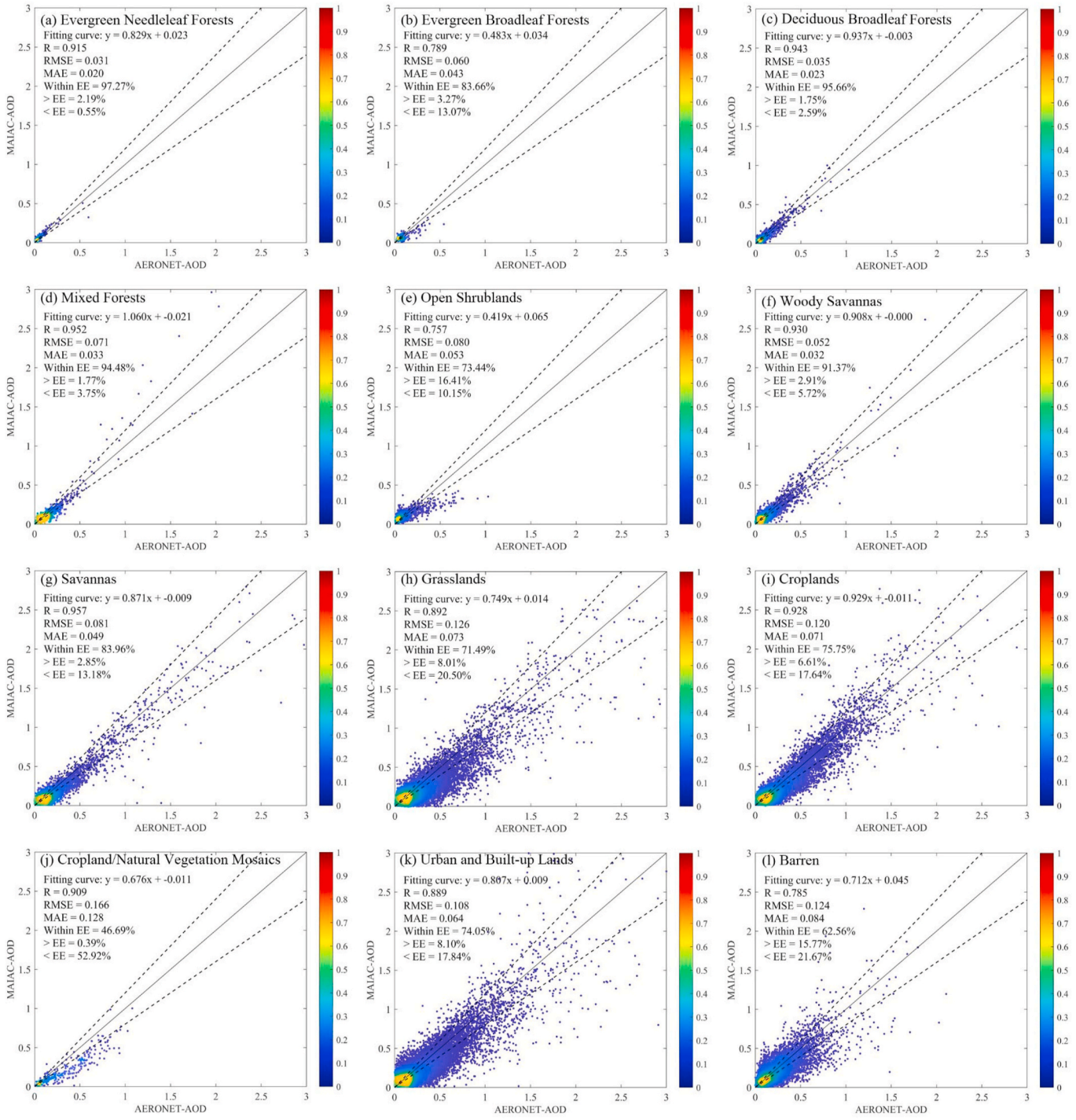

Fig. 7. The verification indexes of MAIAC AOD retrievals for different land-cover-types.

the surface bidirectional reflectance distribution function (BDRF) and aerosols retrieved capabilities in the blue band (Kaufman et al., 1997). MAIAC AOD retrievals performed better over Savannas covers (Fig. 7g) than that over croplands (Fig. 7i) and grassland (Fig. 7h). However, MAIAC AOD retrievals are slightly overestimated (>EE = 16.41% and < EE = 10.15%) under the open shrublands (Fig. 7e) (within EE = 73.44%, RMSE = 0.08 and MAE = 0.053). A poor matchup points within the EE (62.56%) is achieved in areas covered by barrens (Fig. 7l) with high RMSE (0.124) and MAE (0.084) values, because shrublands and barren covers are arid climate characteristics with low vegetation coverage (sand, gravel and drought-resistant plants, etc.).

Especially, an underestimation phenomenon (<EE = 52.93%) is found in regions by cropland/natural vegetation mosaics (Fig. 7j) with RMSE of 0.166 and MAE of 0.128, and only 46.69% of the matchup points falling within the EE. The reason may be that the growth and harvesting period would cause dramatic changes in the surface

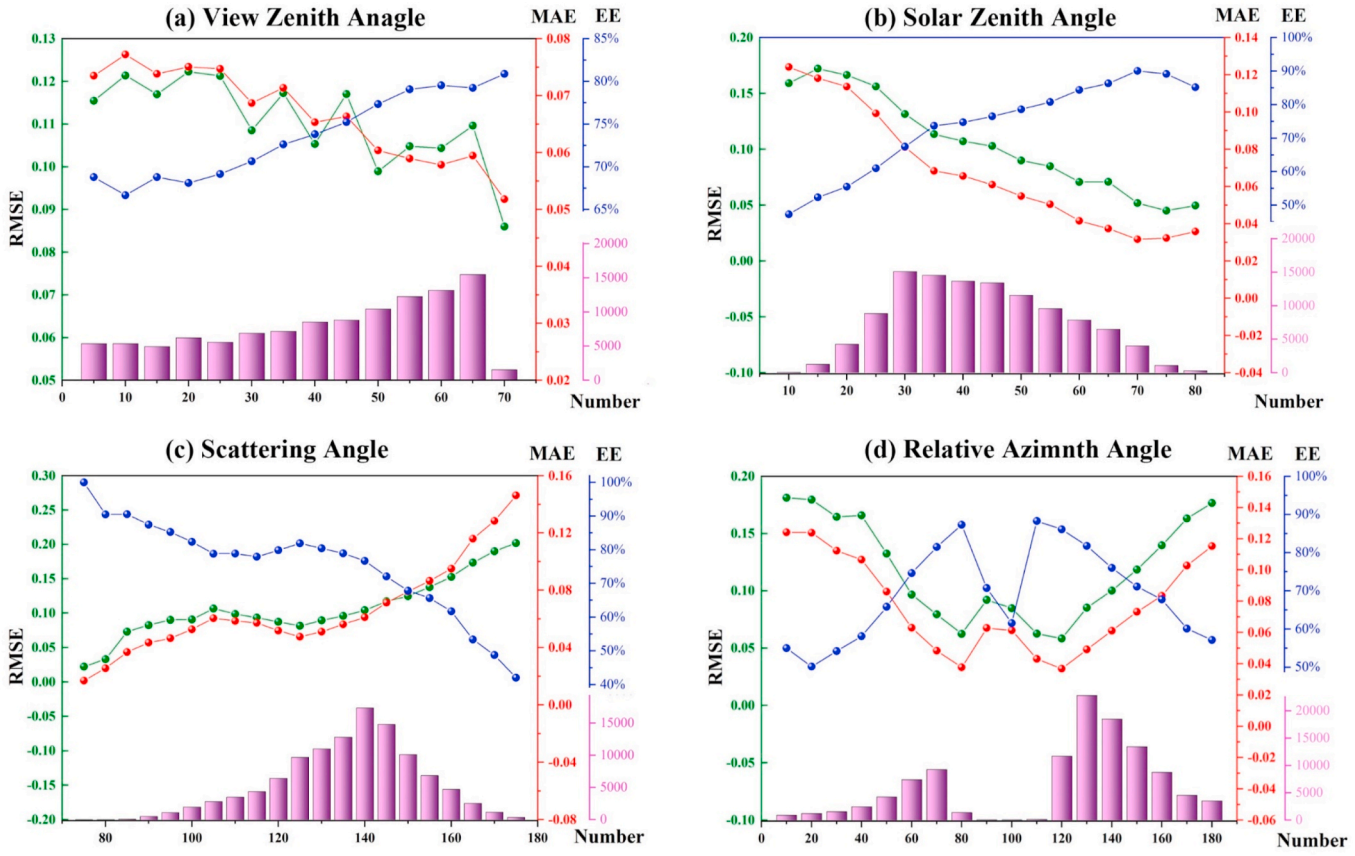

Fig. 8. View geometry dependence of AOD retrievals uncertainty of MAIAC algorithms.

characteristics, which may pose a certain problem to the aerosol retrieval process (Lyapustin and Wang, 2007; Martins et al., 2017). MAIAC algorithm has been improved in aerosol retrieval over bright surface (urban and built-up lands) with 74% of the matchups falling within the EE envelope (Fig. 7k), but still exist a certain deviation (RMSE = 0.108, MAE = 0.064). There may be two reasons for these deviations: (1) the city has a variety of anthropogenic emission sources, which make the aerosol species complex and high concentration; (2) Buildings and roads are typical bright surfaces. The brighter surface cause scattering difference, which leads to the angle dependence of SRC (Martins et al., 2017). The performance of MAIAC AOD retrievals over bright surfaces is worse than that over the dark surface, but still much better than the product provided by the DT or DB algorithm.

3.2.3. View geometry and aerosol conditions dependence of aerosol retrievals

The uncertainty of satellite retrievals is closely related to the view geometry of the solar and the satellites. Here, the effect of four geometric angles including the VZA, SZA, SA and RAA on the accuracy of MAIAC AOD retrievals are analyzed (Fig. 8). RAA was binned into bin size of 10°; VZA, SZA and SA are binned into bin size of 5°. The uncertainty of MAIAC algorithms is calculated for each bin. The uncertainty of MAIAC AOD retrievals varies with the size of VZA. With the increase of VZA (5° ≤ VZA ≤70°), RMSE and MAE show a decreasing trend, while the value of EE gradually increases. Similarly, SZA also shows the same trend as VZA. As SZA increases (10°≤ SZA ≤80°), the uncertainty of the algorithm decreases. On the contrary, the RMSE, MAE tends to be increased and EE tends to be decreased at higher SA (75° ≤ SA ≤ 155°). In general, the size of different SA has a certain impact on aerosol retrieval. Different observation angles cause changes in surface brightness, so the surface reflectance anisotropy influence the accuracy of aerosol retrievals. Furthermore, the backward scattering angle (RAA <90°) surface is usually brighter than the forward scattering angle (RAA >90°) (Roujean et al., 1992). The potential dependence of the MAIAC AOD retrievals on geometry could be changed by considering the changes in surface anisotropy. The inherent limitation of MODIS orbit leads to less sample data obtained within the range of 90° <RAA ≤110° (Superczynski et al., 2017), which in turn causes a small number of the matching points fall into the EE. The mean RMSE (0.128) and MAE (0.08) for the backscattering angle (RAA <90°) are greater than the mean RMSE (0.09) and MAE (0.058) of the forward scattering angle (RAA >90°). On the contrary, the average EE of the backscatter angle (66.37%) is less than the average EE of the forward scattering angle (76.06%). It demonstrates that estimation error of AOD retrievals for the backward scattering angle is larger than that for the forward scattering (see Fig. 9).

MAIAC AOD retrievals show very small positive biases (AOD bias = 0.0038) and small quartile range with a slight overestimation when the AOD loading is lower than 0.4. As the aerosol loading increases (0.4 ≤ AOD ≤1.6), the overall AOD retrievals accuracy decreases. It is worth noting that there is a large bias (AOD $bias_{max}$ = 0.29) under high aerosol loading conditions (AOD ≥1.6), because the formation, source and

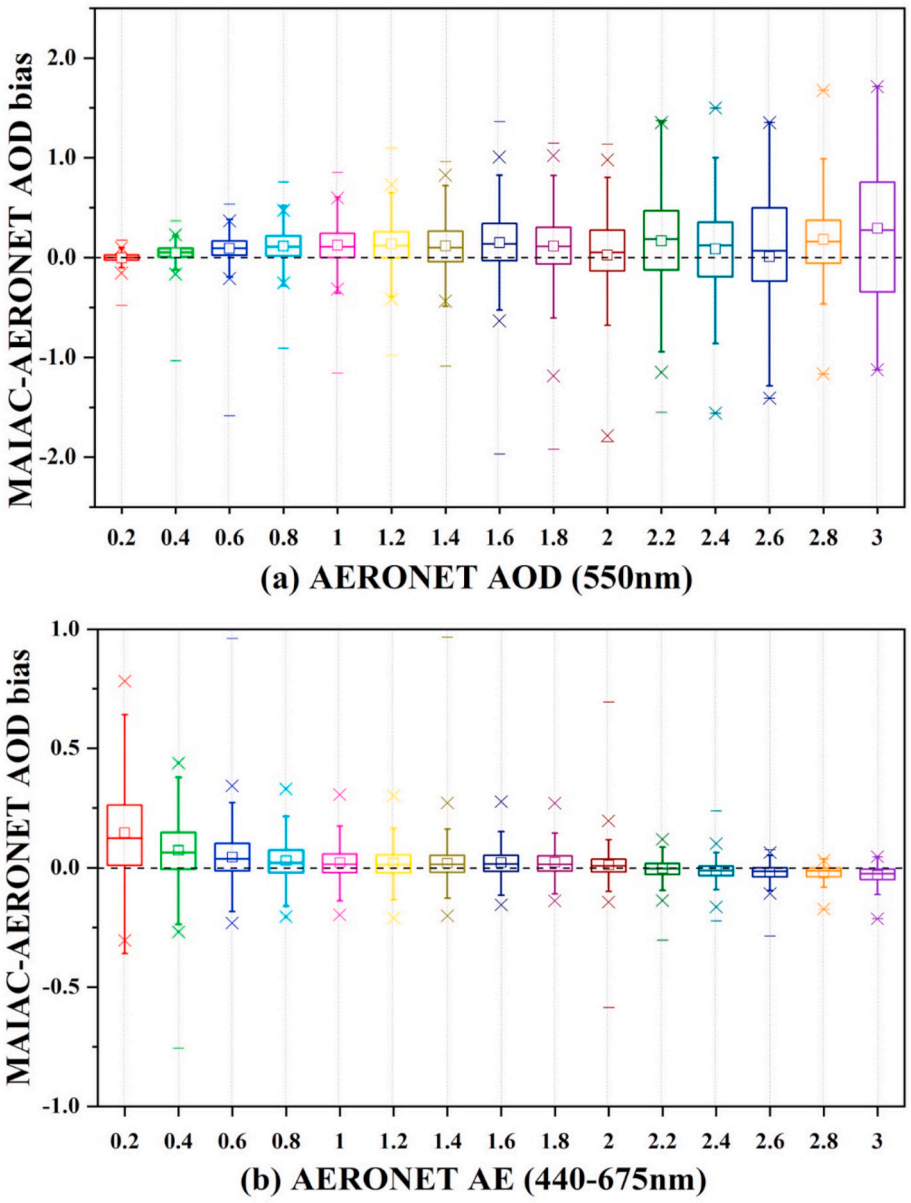

Fig. 9. Box plot of MODIS MAIAC AOD bias with respect to AERONET (a) AOD (550 nm) and (b) AE (440–675 nm) observations. The gray horizontal dashed line represents zero bias. For each box, the middle line, and upper and lower range of the box represent the median, mean, and 25th and 75th percentiles, respectively. The whiskers extend to 1.5 times the interquartile range (IQR).

composition of aerosols are extremely complicated under high aerosol loading conditions. Meanwhile, aerosols are also susceptible to the secondary chemical changes due to the influence of the atmospheric environment (Zheng et al., 2002). The overall results show that the uncertainty of MAIAC algorithm increases with the AOD loading. For coarse aerosol particles (e.g., mineral dust, AE $\leq$ 0.8), the results indicate high positive biases (mean of AOD bias = 0.073) and large quartile range. However, for mixed mode (mixed aerosols containing fine and coarse aerosols, 0.8 < AE $\leq$ 1.4), small sized aerosol particles (1.4 < AE $\leq$ 2.2) and fine aerosol particles (AE $\geq$ 2.2) and fine aerosol particles (AE $\geq$ 2.2), the biases gradually decrease with an overall stable accuracy (mean of AOD bias = 0.018). It also indicates that the aerosol size will affect the retrieval accuracy of MAIAC algorithm.

3.3. Spatial and temporal variation of MAIAC AOD retrievals

Fig. 10 shows the spatial distribution of the annual average values of MAIAC AOD retrievals from 2000 to 2019. The result indicates that aerosol loading presents obvious regional differences on global scale. In order to support the results of this study, the extinction aerosol optical thickness for dust, sea salt, black carbon, SO_4 and organic carbon derived from the Modern-Era Retrospective Analysis for Research and Applications, version 2 (MERRA2) was used. More details can be found in the supplementary materials. Relatively higher AOD values are mainly distributed in China (southern China, Taklimakan desert and north China plain, etc.) Because southern China and north China plain are economically developed and densely populated, leading to a large amount of anthropogenic aerosol emissions (Qin et al., 2018). Fig.S3 and Fig.S4 shows that both black carbon aerosol and SO_4 aerosol optical thickness are high in the north China Plain. The AOD values are also high in central and northern Africa because of the accumulation of dust aerosols transported by the northern Sahara Desert. India is also the area with high annual AOD values. Relatively lower AOD values are widely distributed in Oceania, Europe, southern South America and the Tibetan

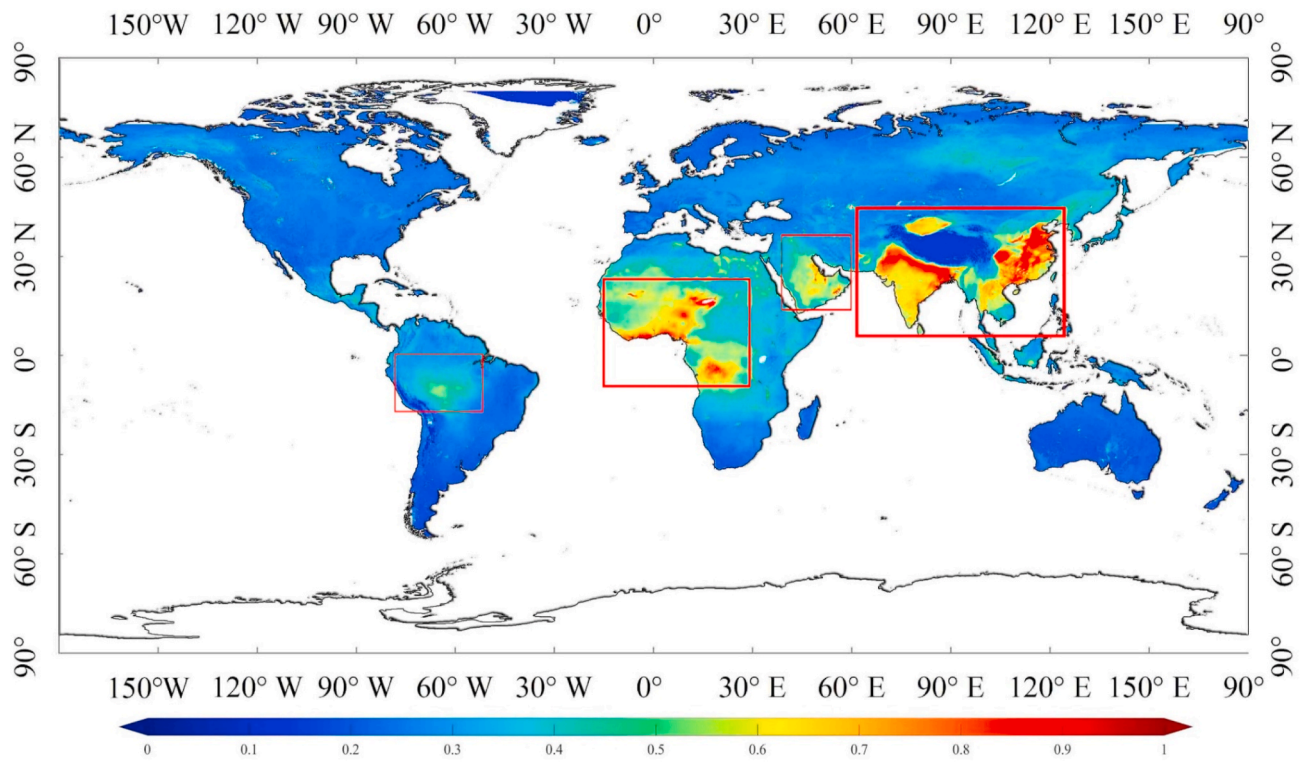

Fig. 10. Spatial distribution of the annual average values of MAIAC AOD retrievals.

Plateau. The reason could be that Oceania is mostly distributed as oceanic aerosols (Fig.S2) with low concentrations (Kaufman et al., 2002). The AOD values are also low in the Tibetan Plateau is due to its less human activities and thin atmosphere (Fang et al., 2021).

Fig. 11 and Fig. 12 show the spatial distribution of the monthly average AOD values during 2000–2019. The seasonal variation of AOD in the northern hemisphere is more obvious than that in the southern hemisphere. The AOD values are high in all the months over north China plain, especially in spring. This can be largely explained that the north China Plain is not only densely populated, but is also a main wheat growing area, indicating a large number of anthropogenic aerosol, straw burning in spring leads to a large number of biomass burning pollutants (Mao and Jin, 2021). High aerosol values are also found in India in all the months. With the development of industrialization in India, coupled with the large population base, a large number of anthropogenic aerosols (such as mining dust and industrial aerosols) have been produced, resulting in high aerosols loading. Similarly, Fig.S3 shows the high value of black carbon aerosol in India. Another interesting phenomenon is that aerosol loading is high from August to October in Brazil, owing to the existence of high intensity forests and biomass burning in Brazil during this period (Ogugbuaja and Barsisa, 2001).

Table 5 shows four statistical indicators of annual AOD values in different climatic type zones. In order to avoid the influence of outliers, this study uses the AOD values in the 99% confidence interval to calculate the annual minimum, maximum, mean and STD in different climatic zones (Table 5). Significant differences of aerosol loading are observed in each climate zones. High annual mean AOD values (0.21, 0.23, 0.19 and 0.24, respectively) are found in climate zone dominated by Am, Aw, BW and Cw. Among them, the climatic zones dominated by Aw and Cw have greater variety of AOD values (STD = 0.11 and 0.15). However, lower annual mean AOD values are observed in regions with polar climates (EF and ET). Although the global AOD values fluctuate in different climate zones, global aerosol values generally remain stable (STD = 0.07), the annual mean AOD values is around 0.15.

4. Conclusion

In this study, MODIS MAIAC AOD product (1 km) was comprehensively evaluated on the global scale. The AOD measurements at 332 AERONET sites are used to verify the performance of MAIAC AOD product in various climate zones, land-cover-types, angular dependence and aerosol conditions. Meanwhile, the spatial and temporal characteristics of AOD over the world are also investigated.

Generally, MAIAC AOD product has good continuity. However, the AOD records are severely missing in high latitude area of northern hemisphere. These areas covered with snow in winter or all the year round, making it impossible to retrieve aerosol optical properties. The performance of MAIAC AOD product show certain differences on the site scale. The small uncertainty of MAIAC AOD retrievals (RMSE <0.1) are found in 75% of the sites. Most of the sites with poor performance of retrievals are basically concentrated in northern Africa and southeastern Asia (RMSE >0.18 and MAE >0.16). The high accuracy is mainly achieved in the regions of tropical rainforest climate and tropical open forest climate (within EE = 87.49% and 83.15%, RMSE = 0.05 and 0.05, MAE = 0.04 and 0.05). However, for regions dominated by the polar climate (EF, ET), the accuracy is poor (RMSE = 0.14 and 0.12). The accuracy of MAIAC algorithm also depends on land-cover-types. The results show that the satisfactory accuracy always appears in the forest,

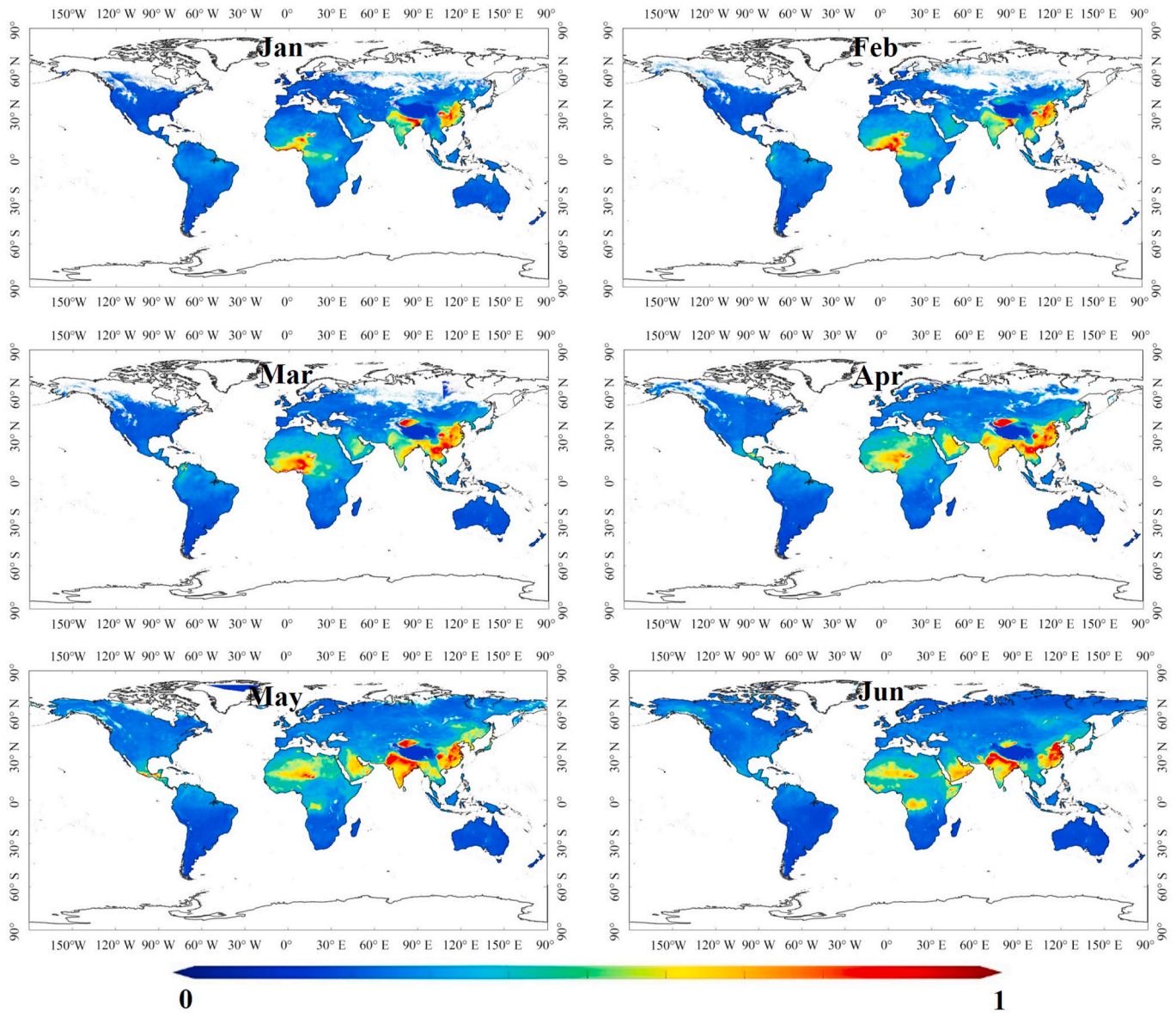

Fig. 11. Spatial distribution of monthly average of MAIAC AOD product.

with the fraction within EE varying from 73.44 to 97.27% and R between 0.87 and 0.98. Followed by croplands, Urban and Built-up Lands and barren, the RMSE of 0.108 and 0.124 and MAE of 0.084 and 0.064 are obtained on the bright surface (Urban and Built-up Lands and barren). The performance of Cropland/Natural Vegetation Mosaics is the worst (within EE = 46.69%, RMSE = 0.166 and MAE = 0.128).

Aerosol conditions also affect the quality of MAIAC AOD retrievals. The result shows that a poorer performance of MAIAC algorithm appears when the aerosol loading increases with small AE. The changes of the geometric angles of the solar and satellites also cause some inherent uncertainties. The results show that the bias for the backward scattering angle (RAA $<90°$) is larger than that of the forward scattering angle (RAA $>90°$), which indicates that MAIAC algorithm has higher accuracy and less dependence on forward scattering angle. Changes in the size of VZA, SZA and SA all affect the results of MAIAC AOD retrievals. Finally, the spatial and temporal distribution of AOD values was investigated on global scale. The high AOD values are mainly distributed in China (southern China, Taklimakan desert and north China plain), central Africa and India, while the low AOD values are widely distributed in Oceania, Europe, southern South America and the Tibetan Plateau.

Declaration of competing interest

The authors declare that they have no known competing financial interests or personal relationships that could have appeared to influence the work reported in this paper.

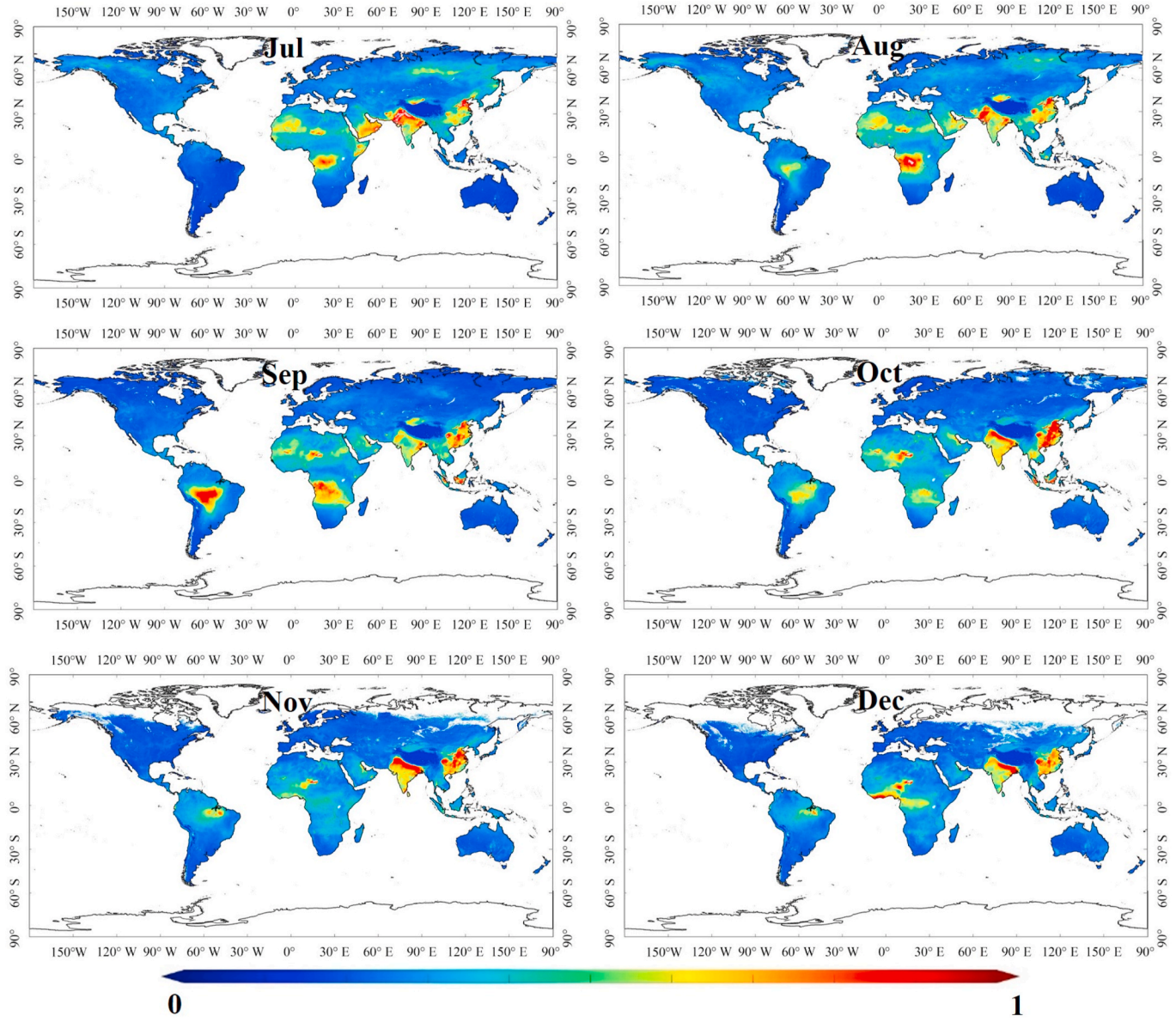

Fig. 12. Spatial distribution of monthly average of MAIAC AOD product.

Table 5
The annual minimum, maximum, mean and standard deviation (STD) AOD values of 99% confidence intervals in different climatic type zones.

Climate classification	Minimum	Maximum	Mean	STD
Af	0.08	0.36	0.17	0.06
Am	0.05	0.53	0.21	0.09
Aw	0.07	0.57	0.23	0.11
BS	0.01	0.52	0.14	0.08
BW	0.01	0.56	0.19	0.10
Cf	0.05	0.64	0.14	0.13
Cs	0.05	0.29	0.11	0.03
Cw	0.01	0.66	0.24	0.15
Df	0.08	0.23	0.12	0.03
Ds	0.01	0.23	0.12	0.03
Dw	0.01	0.59	0.16	0.08
EF	0.00	0.19	0.01	0.04
ET	0.00	0.18	0.09	0.02
Global	0.03	0.43	0.15	0.07

Acknowledgements

This work was financially supported by National Natural Science Foundation of China (No. 42001016), the Special Fund for Basic Scientific Research of Central Colleges, China University of Geosciences, Wuhan (No. 111-162301182738). We would like to thank the NASA Earth data website (https://search.earthdata.nasa.gov/search) for providing MODIS aerosol and auxiliary products and the NASA Goddard Space Flight Center (https://aeronet.gsfc.nasa) for providing AERONET ground measurements.

Appendix A. Supplementary data

Supplementary data to this article can be found online at https://doi.org/10.1016/j.atmosenv.2021.118684.

Authorship contributions

Wenmin Qin, Conception and design of study, Drafting the manuscript, Approval of the version of the manuscript to be published, Hejin

Fang, Conception and design of study, Drafting the manuscript, Approval of the version of the manuscript to be published, Lunche Wang, Conception and design of study, Acquisition of data, Revising the manuscript critically for important intellectual content, Approval of the version of the manuscript to be published, Jing Wei, Acquisition of data, Drafting the manuscript, Approval of the version of the manuscript to be published, Ming Zhang, Acquisition of data, Revising the manuscript Critically for important intellectual content, Approval of the version of the manuscript to be published, Xin Su, Formal analysis and/or interpretation of data, Drafting the manuscript, Approval of the version of the manuscript to be published, Muhammad Bilal, Acquisition of data, Revising the manuscript critically for important intellectual content, Approval of the version of the manuscript to be published, Xun Liang, Formal analysis and/or interpretation of data, Revising the manuscript critically for important intellectual content, Approval of the version of the manuscript to be published,

References

Ångström, A., 1929. On the atmospheric transmission of sun radiation and on dust in the air. Geogr. Ann. 11, 156–166.

Banerjee, T., Kumar, M., Mall, R.K., Singh, R.S., 2017. Airing 'clean air' in clean India mission. Environ. Sci. Pollut. Control Ser. 24, 6399–6413.

Chudnovsky, A., Tang, C., Lyapustin, A., Wang, Y., Schwartz, J., Koutrakis, P., 2013. A critical assessment of high-resolution aerosol optical depth retrievals for fine particulate matter predictions. Atmos. Chem. Phys. 13, 10907–10917.

Emili, E., Lyapustin, A., Wang, Y., Popp, C., Korkin, S., Zebisch, M., Wunderle, S., Petitta, M., 2011. High spatial resolution aerosol retrieval with MAIAC: application to mountain regions. J. Geophys. Res.: Atmosphere 116.

Evans, J., van Donkelaar, A., Martin, R.V., Burnett, R., Rainham, D.G., Birkett, N.J., Krewski, D., 2013. Estimates of global mortality attributable to particulate air pollution using satellite imagery. Environ. Res. 120, 33–42.

Fang, H., Qin, W., Wang, L., Zhang, M., Yang, X., 2021. Solar brightening/dimming over China's mainland: effects of atmospheric aerosols, anthropogenic emissions, and meteorological conditions. Rem. Sens. 13.

Gengrui, Z., Yu, L., 2015. Types and changes of Chinese climate zones from 1961 to 2013 based on Köppen climate classification. Arid. Land Geogr. 38, 1121–1132.

Holben, B.N., Eck, T.F., Slutsker, I., Tanré, D., Buis, J.P., Setzer, A., Vermote, E., Reagan, J.A., Kaufman, Y.J., Nakajima, T., Lavenu, F., Jankowiak, I., Smirnov, A., 1998. AERONET—a federated instrument network and data archive for aerosol characterization. Rem. Sens. Environ. 66, 1–16.

Holben, B.N., Tanré, D., Smirnov, A., Eck, T.F., Slutsker, I., Abuhassan, N., Newcomb, W. W., Schafer, J.S., Chatenet, B., Lavenu, F., Kaufman, Y.J., Castle, J.V., Setzer, A., Markham, B., Clark, D., Frouin, R., Halthore, R., Karneli, A., O'Neill, N.T., Pietras, C., Pinker, R.T., Voss, K., Zibordi, G., 2001. An emerging ground-based aerosol climatology: aerosol optical depth from AERONET. J. Geophys. Res.: Atmosphere 106, 12067–12097.

Hsu, N.C., Si-Chee, T., King, M.D., Herman, J.R., 2004. Aerosol properties over bright-reflecting source regions. IEEE Trans. Geosci. Rem. Sens. 42, 557–569.

Jackson, J.M., Liu, H., Laszlo, I., Kondragunta, S., Remer, L.A., Huang, J., Huang, H.-C., 2013. Suomi-NPP VIIRS aerosol algorithms and data products. J. Geophys. Res.: Atmosphere 118 (12), 673-612,689.

Kahn, R.A., Gaitley, B.J., Garay, M.J., Diner, D.J., Eck, T.F., Smirnov, A., Holben, B.N., 2010. Multiangle imaging SpectroRadiometer global aerosol product assessment by comparison with the aerosol robotic network. J. Geophys. Res.: Atmosphere 115.

Kaufman, Y.J., Tanré, D., Boucher, O., 2002. A satellite view of aerosols in the climate system. Nature 419, 215–223.

Kaufman, Y.J., Wald, A.E., Remer, L.A., Bo-Cai, G., Rong-Rong, L., Flynn, L., 1997. The MODIS 2.1-/spl mu/m channel-correlation with visible reflectance for use in remote sensing of aerosol. IEEE Trans. Geosci. Rem. Sens. 35, 1286–1298.

Kumar, M., Singh, R.S., Banerjee, T., 2015. Associating airborne particulates and human health: exploring possibilities: comment on: kim, Ki-Hyun, Kabir, E. and Kabir, S. 2015. A review on the human health impact of airborne particulate matter, 2015 Environ. Int. 74, 136–143. Environ Int 84, 201-202.

Lee, S., Pinhas, A., Alexei, L., Yujie, W., Alexandra, C.A., 2017. An example of aerosol pattern variability over bright surface using high resolution MODIS MAIAC: the eastern and western areas of the Dead Sea and environs (Oxford, England : 1994). Atmos. Environ. 165, 359–369.

Levy, R.C., Mattoo, S., Munchak, L.A., Remer, L.A., Sayer, A.M., Patadia, F., Hsu, N.C., 2013. The Collection 6 MODIS aerosol products over land and ocean. Atmos. Meas. Tech. 6, 2989–3034.

Lyapustin, A., Korkin, S., Wang, Y., Quayle, B., Laszlo, I., 2012. Discrimination of biomass burning smoke and clouds in MAIAC algorithm. Atmos. Chem. Phys. 12, 9679–9686.

Lyapustin, A., Wang, Y., 2007. MAIAC-Multi-Angle Implementation of Atmospheric Correction for MODIS. AGU Spring Meeting Abstracts. A51B-05.

Lyapustin, A., Wang, Y., Frey, R., 2008. An automatic cloud mask algorithm based on time series of MODIS measurements. J. Geophys. Res.: Atmosphere 113.

Lyapustin, A., Wang, Y., Korkin, S., Huang, D., 2018. MODIS Collection 6 MAIAC algorithm. Atmospheric Measurement Techniques 11, 5741–5765.

Lyapustin, A., Wang, Y., Laszlo, I., Kahn, R., Korkin, S., Remer, L., Levy, R., Reid, J.S., 2011. Multiangle implementation of atmospheric correction (MAIAC): 2. Aerosol algorithm. J. Geophys. Res. 116.

Mao, Q., Jin, S., 2021. Research on the spatial and temporal distribution characteristics of global aerosol optical depth from 2009 to 2018. Laser & Optoelectronics Progress 58, 1–9.

Martins, V.S., Lyapustin, A., de Carvalho, L.A.S., Barbosa, C.C.F., Novo, E.M.L.M., 2017. Validation of high-resolution MAIAC aerosol product over South America. J. Geophys. Res.: Atmosphere 122, 7537–7559.

Mhawish, A., Banerjee, T., Broday, D.M., Misra, A., Tripathi, S.N., 2017. Evaluation of MODIS Collection 6 aerosol retrieval algorithms over Indo-Gangetic Plain: implications of aerosols types and mass loading. Rem. Sens. Environ. 201, 297–313.

Mhawish, A., Banerjee, T., Sorek-Hamer, M., Lyapustin, A., Broday, D.M., Chatfield, R., 2019. Comparison and evaluation of MODIS multi-angle implementation of atmospheric correction (MAIAC) aerosol product over South Asia. Rem. Sens. Environ. 224, 12–28.

Ogugbuaja, V.O., Barsisa, L.Z., 2001. Atmospheric pollution in North-East Nigeria: measurement and analysis of suspended particulate matter. Bull. Chem. Soc. Ethiop. 15, 109–117.

Peel, M.C., Finlayson, B.L., McMahon, T.A., 2007. Updated world map of the Köppen-Geiger climate classification. Hydrol. Earth Syst. Sci. 11, 1633–1644.

Pope Iii, C.A., Burnett, R.T., Thun, M.J., Calle, E.E., Krewski, D., Ito, K., Thurston, G.D., 2002. Lung cancer, cardiopulmonary mortality, and long-term exposure to fine particulate air pollution. J. Am. Med. Assoc. 287, 1132–1141.

Qin, W.M., Liu, Y., Wang, L.C., Lin, A.W., Xia, X.G., Che, H.Z., Bilal, M., Zhang, M., 2018. Characteristic and driving factors of aerosol optical depth over mainland China during 1980-2017. Rem. Sens. 10.

Ramanathan, V., Ramana, M.V., 2005. Persistent, widespread, and strongly absorbing haze over the himalayan foothills and the indo-gangetic plains. Pure Appl. Geophys. 162, 1609–1626.

Roujean, J.-L., Leroy, M., Deschamps, P.-Y., 1992. A bidirectional reflectance model of the Earth's surface for the correction of remote sensing data. J. Geophys. Res.: Atmosphere 97, 20455–20468.

Seinfeld, J.H., Bretherton, C., Carslaw, K.S., Coe, H., DeMott, P.J., Dunlea, E.J., Feingold, G., Ghan, S., Guenther, A.B., Kahn, R., Kraucunas, I., Kreidenweis, S.M., Molina, M.J., Nenes, A., Penner, J.E., Prather, K.A., Ramanathan, V., Ramaswamy, V., Rasch, P.J., Ravishankara, A.R., Rosenfeld, D., Stephens, G., Wood, R., 2016. Improving our fundamental understanding of the role of aerosol−cloud interactions in the climate system. Proc. Natl. Acad. Sci. Unit. States Am. 113, 5781.

Smirnov, A., Holben, B.N., Eck, T.F., Dubovik, O., Slutsker, I., 2000. Cloud-screening and quality control algorithms for the AERONET database. Rem. Sens. Environ. 73, 337–349.

Su, X., Wang, L., Zhang, M., Qin, W., Bilal, M., 2021. A high-precision aerosol retrieval algorithm (HiPARA) for advanced Himawari imager (AHI) data: development and verification. Rem. Sens. Environ. 253, 112221.

Superczynski, S.D., Kondragunta, S., Lyapustin, A.I., 2017. Evaluation of the multi-angle implementation of atmospheric correction (MAIAC) aerosol algorithm through intercomparison with VIIRS aerosol products and AERONET. J. Geophys. Res.: Atmosphere 122, 3005–3022.

Tao, M., Wang, J., Li, R., Wang, L., Wang, L., Wang, Z., Tao, J., Che, H., Chen, L., 2019. Performance of MODIS high-resolution MAIAC aerosol algorithm in China: characterization and limitation. Atmos. Environ. 213, 159–169.

Wei, J., Li, Z., Pinker T., R., Sun, L., Li, R., 2021. Himawari-8-derived diurnal variations of ground-level PM2.5 pollution across China using a fast space-time Light Gradient Boosting Machine. Atmos. Chem. Phys. 21 (10), 7863–7880.

Wei, J., Sun, L., Peng, Y., Wang, L., Zhang, Z., Bilal, M., Ma, Y., 2018. An improved high-spatial-resolution aerosol retrieval algorithm for MODIS images over land. J. Geophys. Res.: Atmosphere 123 (12), 291-212,307.

Yoshida, M., Kikuchi, M., Nagao, T.M., Murakami, H., Nomaki, T., Higurashi, A., 2018. Common retrieval of aerosol properties for imaging satellite sensors. Journal of the Meteorological Society of Japan. Ser. II 96B, 193–209 advpub).

Zhang, H., Kondragunta, S., Laszlo, I., Zhou, M., 2020. Improving GOES Advanced Baseline Imager (ABI) aerosol optical depth (AOD) retrievals using an empirical bias correction algorithm. Atmos. Meas. Tech. 13, 5955–5975.

Zhang, Z., Wu, W., Fan, M., Wei, J., Tan, Y., Wang, Q., 2019. Evaluation of MAIAC aerosol retrievals over China. Atmos. Environ. 202, 8–16.

Zheng, M., Cass, G.R., Schauer, J.J., Edgerton, E.S., 2002. Source apportionment of PM2.5 in the southeastern United States using solvent-extractable organic compounds as tracers. Environ. Sci. Technol. 36, 2361–2371.